Korean J. Chem. Eng., 40(8), 1822-1838 (2023)
DOI: 10.1007/s11814-023-1455-6

pISSN: 0256-1115
eISSN: 1975-7220

REVIEW PAPER

TiO_2 based nanomaterial: Synthesis, structure, photocatalytic properties, and removal of dyes from wastewater

Sanjeev Kumar† and Avaani Chanana

Applied Science Cluster, Department of Chemistry, University of Petroleum and Energy Studies, Dehradun
(*Received 31 October 2022 • Revised 8 March 2023 • Accepted 19 March 2023*)

Abstract−Owing to its complex chemical makeup, dye pollution from the textile sector poses a serious challenge for wastewater. Using a photocatalyst with light irradiation to remove color from wastewater is a potential wastewater treatment technique. The majority of harmful dyes are resistant to biodegradation, which reduces the effectiveness of biological wastewater treatment facilities. A well-known photocatalyst for wastewater treatment, titanium dioxide is typically utilized in suspensions in photoreactions. TiO_2 based nanomaterial offers some benefits over other materials, including its inexpensive cost, low toxicity, high photochemical reactivity, and capacity for generalized oxidative attack. By doing so, it can encourage the breakdown of certain target organic molecules while just slightly altering operational parameters. The aim of this review is to highlight the different method for synthesis and its characterization. This review also highlights the different type of TiO_2/composite as photocatalyst for removal of dyes. The general mechanism of photocatalytic effect of TiO_2 has been discussed expansively. This paper takes a thorough approach to the many outcomes of the researchers' efforts to remove dyes from wastewater.

Keywords: TiO_2, Photocatalyst, Synthesis, Mechanism, Dyes, Wastewater

INTRODUCTION

One of the most valuable and irreplaceable resources known is water. Water consumption per person varies considerably between nations, and home, industrial, and public uses all contribute to the issue of widespread water mismanagement [1]. The pollution of wastewater brought on by expanding industry in recent years is becoming more and more recognized. Industrial wastewater from the paper and textile industries, in particular, contains a complex mixture of different organic compounds, heavy metals, and azo-dyes that are difficult to remove in natural environments because of their high solubility, stability, and low biodegradability in aqueous media [2]. The presence of organic contaminants in industrial water and wastewater is seen as a serious issue for people everywhere. There is an increase in water and air pollution. Pharmaceutical, tannery, and textile industries all colored effluent, and these businesses use synthetic dyes and pigments extensively [3-7]. Particularly in the textile manufacturing sector, 10 to 50 percent of the dye that is used during the dying process is lost and discharged in the effluent [8-10]. The textile industries let out wastewater that has high pH, foul smell, high BOD (biological oxygen demand), acids, bases and heavy metals that are toxic for the environment [11]. In addition, dyes accumulating in water damage the aesthetics of the environment. A majority of dyes are stable and resistant to oxidation, light, and aerobic degradation for a long time. Azo-dyes are poisonous, obstruct the passage of light, and stop the growth of vegetation and fauna in bodies of water. Additionally, given that the azo group (N=N) is transformed into aromatic amines, which have the potential to induce human cancer, some dyes and the byproducts of their breakdown can be viewed as potential pollutants [2,12]. The dyes in effluents must therefore be removed before they are discharged into water reservoirs. Different methods have been tested to remove toxicity from water, including photocatalytic degradation, UV irradiation, membrane filtration, osmosis, microextraction, and nanofiltration [13,14]. In spite of the extensive study of these methods, they have some drawbacks, such as high capital costs, the need for chemicals, their ineffectiveness to remove all pollutants, and the fact they do not destroy the pollutants [8,15]. Advanced oxidation processes (AOP) can degrade organic compounds that are resistant to conventional treatment methods. When the pollutants contain halogens, AOP releases reactive species, mainly hydroxyl radicals that help break down the target molecule, generating CO_2, H_2O, and mineral acids [8,16]. Photocatalytic degradation techniques can be used to degrade organic pollutants and textile dyes, and semiconductor catalyst have been used for this technique [17]. Photocatalysis is an advanced oxidation process that is used to remove the pollutants from wastewater with the help of semiconductor catalyst, and UV light and photocatalyst have the potential to convert light energy to chemical energy [18]. The creation of more effective photocatalyst materials has been the focus of significant research since Fujushima and colleagues' groundbreaking work on titanium-based photocatalysis in the early 1970s [19,20]. Titania-based photocatalyst materials have been applied to a wide range of environmental remediation and water contamination applications [19-22], as well as solar cell materials [19,21,23], hydrogen production from water [19,23,24], organic synthesis processes [19,25,26], anti-fog, and antimicrobial solutions [19,27,28], etc. Due to its excellent photocatalytic activity, chemical stability, non-toxicity, and via-

†To whom correspondence should be addressed.
E-mail: sanjeevkumar.dubey2@gmail.com

bility from an economic standpoint, nano TiO_2 has been employed extensively as a photocatalyst for dye degradation. TiO_2 exclusively absorbs anatase in the UV range and has a high band gap energy (3.2 eV) [3,29-31]. Visible light makes up 46% of solar energy, while UV light makes up only 6%. Therefore, coupled TiO_2 application with external UV irradiation was widely utilized for the treatment of industrial effluent [3,32]. It is expensive and challenging to put the combined UV+TiO_2 treatment process into real-time operation. Reducing the band gap energy from the UV area to the visible light region can be accomplished by doping the TiO_2 particles in the crystalline structure material or by synthesizing TiO_2 composites [3]. TiO_2 has three polymorphic types: brookite (orthorhombic), anatase (tetragonal) and rutile (tetragonal). The anatase TiO_2 has a small size and is the metastable form that helps in photocatalytic activity [33]. Application of TiO_2 nanoparticles include work in the medicinal field and in cancer therapies [34], food preservation, cosmetics [35], and dye synthesized solar cells [36].

In this review, we discuss different methods used for the synthesis of TiO_2 and titania-based material, structural, and morphological studies, photocatalytic degradation and mechanism of degradation of different dyes. We have tabulated many more titania based nanomaterials as photocatalyst which have been able to remove different dyes from wastewater efficiently This review is going to help researchers in many ways for selecting suitable catalysts for water remediation and may enhance the catalytic properties.

SYNTHESIS OF TiO_2 AND TIO_2 BASED MATERIALS

Different photocatalytic materials have been synthesized by many researchers. Qiao et al. synthesized polyglutamic acid functionalized Ag/g-C_3N_4/SiC photocatalyst [37]. Liu et al. prepared polyglycine functionalized gold/iron doped silver iodide for photocatalysis [38]. Bahadoran et al. obtained Co-doping silver and iron on graphitic carbon nitride-carrageenan nanocomposite for the photocatalytic process [39]. Spinel tin ferrite ornamented on Bismuth ferrite nanostructures was created by Xiao et al. [40] as a synergetic photocatalyst. Sn/Fe nanoparticles created by Bahadoran et al. [41] demonstrated excellent photocatalytic performance for the breakdown of methyl orange about 95.1% in 35 minutes. Hydrothermal technique was used by Mao et al. [42] to produce silver Ferrite/Bismuth ferrite nano-hybrids. Using methylene blue dye and visible light illumination, composites' photocatalytic activity was tested. In 120 minutes, the dye had totally broken down.

By using a chemical process, Long et al. [43] created $Ba_{1-x}Ti_xFe_2O_{4+\delta}$ with x ranging from 0.0 to 1.0. The greatest photocatalyst is $Ba_{0.3}Ti_{0.7}Fe_2O_{4.7}$ nanoparticles, which have a 100 percent degra-

Fig. 1. Methods used to synthesize TiO_2 and TiO_2 based materials.

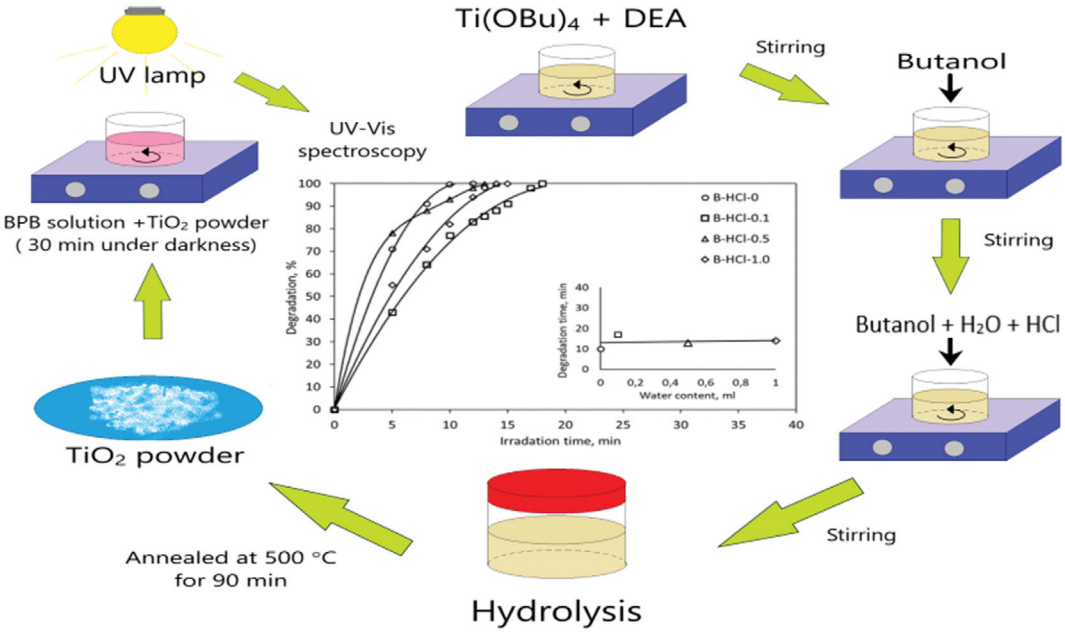

Fig. 2. Schematic diagram of Sol Gel method [66]. Reproduced with permission © 2021 Elsevier B.V. All rights reserved.

dation potential. By using a hydrothermal process, Bahadoran et al. [44] were able to immobilize Ag doped Sn_3O_4 nanostructure on hyperbranched polypyrrole. Under visible light irradiation, the photocatalytic activity of composites was reported to degrade Congo red by 100% in 30 minutes. Copper oxide (CuO) nanorods and cupric tungstate ($CuWO_4$) nanoparticles were made by Cai et al. [45] using the hydrothermal method, and the photocatalytic activity was examined. Akhter et al. [46] synthesized porous Ag_3VO_4/KIT-6 composite for degradation of Congo red. Shabir et al. [47] discussed in a review different method of degradation of dyes with life cycle of assessment. Azam et al. [48] reviewed the role of activated carbon for removal of anionic dyes from waste water. Shehzad et al. [49] elaborated the improvement in effectiveness of TiO_2-based photocatalytic systems by a number of modifications, including metal and non-metal doping, co-photocatalyst, semiconductor coupling, crystal and facet engineering, state-of-the-art morphologies, and novel architectures. But Our review focuss on TiO_2 based nanomaterial. So have given more emphasis on synthesis of TiO_2 based nanomaterial by different route.

Since titanium oxide's physicochemical characteristics, such as its size, shape, morphology, and composition, are crucial to the photocatalytic performance, it is important to control them. To do this, a synthetic process must be used, which can help advance the development of new photocatalytic technologies of the photocatalyst's desirable characteristics. Additionally, the titanium oxides should be produced using a process that is both economically sound and environmentally friendly. To achieve this, a variety of approaches have been tried, some of which are suitable for the production of titanium dioxide and its composites.

TiO_2 nanoparticles can be synthesized easily by different methods. Methods that include-solgel method, electrochemical method, microwave synthesis, solvothermal method, green synthesis techniques, micro emulsion, chemical vapor deposition, physical vapor deposition and sonochemical (Fig. 1).

1. Sol Gel Method

Fig. 2 is a schematic diagram for the sol-gel method. For creating materials with a range of forms, porous structures, thin fibers, dense powders, and thin films, the sol-gel process was created in the 1960s. A system must go from a liquid solution (sol) to a solid gel phase as part of the sol-gel process (gel). A sol is a liquid that contains colloidal particles that are not dissolved but also do not aggregate or settle. A stable dispersion of colloidal particles or polymers in a solvent is referred to as a sol. In contrast to a gel, which is made up of a three-dimensional continuous network that surrounds a liquid phase, a colloidal gel's network is composed of aggregates of colloidal particles [50]. The sol-gel process produces TiO_2 nanoparticles by converting titanium alkoxide into oxopolymers (dehydration and de-alcoholation) and then transforming them into oxide networks. Hydrolysis and polycondensation rate strongly influence metal oxide structure and properties [50]. Lee et al. synthesized the TiO_2 by sol-gel method using titanium isopropoxide (TTIP) [51]. Dubey et al. prepared TiO_2 by sol-gel method in good yield [52]. Ahmad et al. synthesized TiO_2 by sol-gle method using titanium tetra isopropoxide (TTIP) [53]. Hussain et al. [54] synthesized TiO_2 of good surface area. Hussain et al. [55] prepared TiO_2 by sol-gel method for photodegradation of volatile organic compounds (VOC). Rashid et al. [56] synthesized NS/TiO_2 adsorbent by sol-gel method for removal of cationic dyes. Sol gel method is generally used as a method for synthesizing TiO_2 NPs because of the high purity, control over stoichiometry, ambient temperature synthesis and crystallinity, smaller particle size, control morphology, improved homogeneity and Low-temperature sintering [18,57]. Sol-gel precipitating method is a better method for synthesis of nanocomposite because of its distinguishing metastable structure at low temperature, chemical characteristics and very high purity [58].

$TiCl_4$ in ethanol solution can be used as a precursor in the sol

gel method. The reaction is performed under room temperature and stirred continuously, gases like Cl and HCl are evolved, the solution obtained is yellow and is gelatinized for some days to get a sol gel, then dried at a temperature and dried gel is referred to as TiO_2 NPs [59]. Here, the sol-gel method uses distilled water, with adequate proportion of NaOH solution added to the zinc acetate solution with constant stirring which leads to the formation of ZnO. Simultaneously the titanium isopropoxide solution is mixed with ethanol and some water leading to formation of TiO_2. then the two above solutions are stirred for few hours which leads to the formation TiO_2: ZnO composite.

This composite shows high stability and help in reducing the trapped centers on ZnO surface that leads to reducing the photocatalytic activity [60]. The nanocomposite shows type-2 band offset in which the valence band and conduction band of TiO_2 are less than that of ZnO, which leads to separation of holes and photogenerated electrons [61]. Dopants used are non-metals and transition metals which include Zn, Co, N, C, S [62-64]. Doping with transition metals helps in increasing the photocatalytic activity of titania. Zn^{2+} has the most the effective doping with titanium because of same ionic radii and thus the resultant doped nanoparticle obtained is highly effective [65].

The simple way to synthesize Zn doped Ti nanoparticles is by sol-gel method, which is an effective method (Fig. 3).

Dopants used are non-metals and transition metals which include Zn, Co, N, C, S [62-64]. Doping with transition metals helps in increasing the photocatalytic activity of titania. The Zn^{2+} has the most the effective doping with titanium because of same ionic radii and thus the resultant doped nanoparticle obtained is highly effective [65].

2. Electrochemical Method

Fig. 4 shows the electrochemical method for the synthesis of TiO_2. This method can be used to synthesize pure anatase TiO_2 nanoparticles. In this bulk metal is oxidized at anode. The metal cations travel to the cathode; during the preparation the size of particle is decreased by increasing current intensity [68]. The electrolyte used acts as surfactant so that agglomeration does not occur [69].

3. Co-precipitation Method

Titanium dioxide can be synthesized by precipitation method. TiO_2 powder is made using titanium isopropoxide, $C_{12}H_{28}O_4Ti$, as a starting ingredient. The process involves adding 5 ml of titanium isopropoxide drop by drop into 8 ml of deionized water. This causes the alkoxide to hydrolyze and hydrous titanium oxides to precipitate. For 30 minutes, the solution is continuously stirred at 40 °C to ensure thorough mixing. After completing this procedure, a white precipitate of TiO_2 nanoparticles forms at the bottom of the beaker. It is centrifuged out, repeatedly rinsed in deionized water and methanol, and then dried for 12 hours at 80 °C [70]. Nanocomposite Zn doped TiO_2 can also be synthesized by co-precipitation and calcination method in which Zn and Ti salts are used as raw materials [71,72].

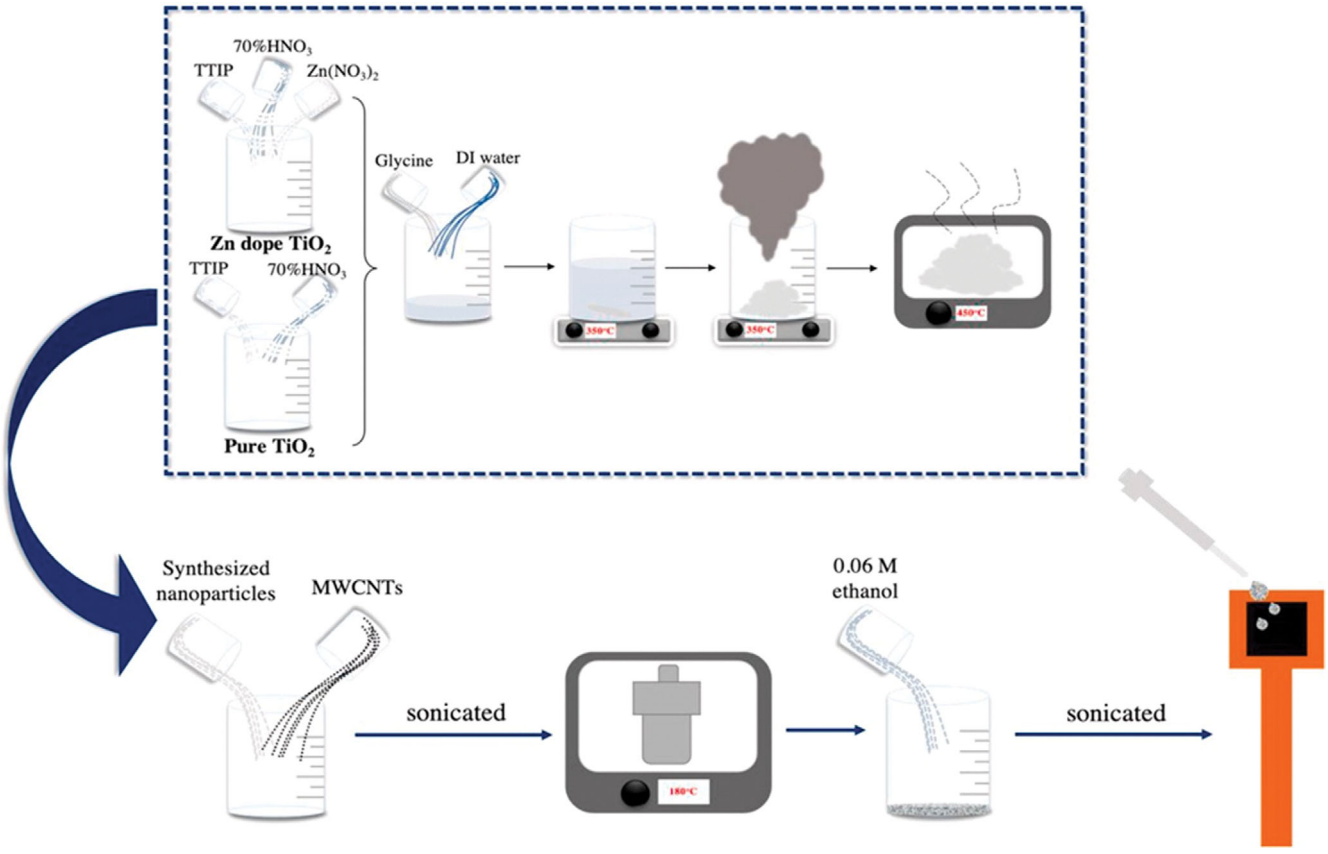

Fig. 3. Preparation of TiO_2 and Zn doped TiO_2 [67] (with permission © 2021 Elsevier Ltd and Techna Group S.r.l.).

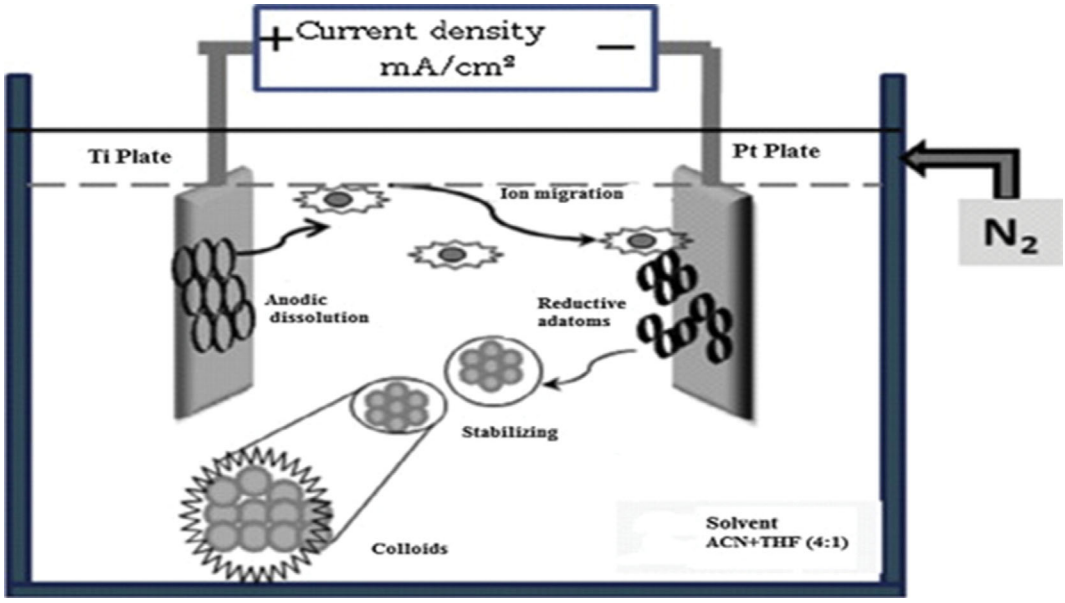

Fig. 4. Electrochemical Method [68] (with permission © 2019 Published by Elsevier B.V.).

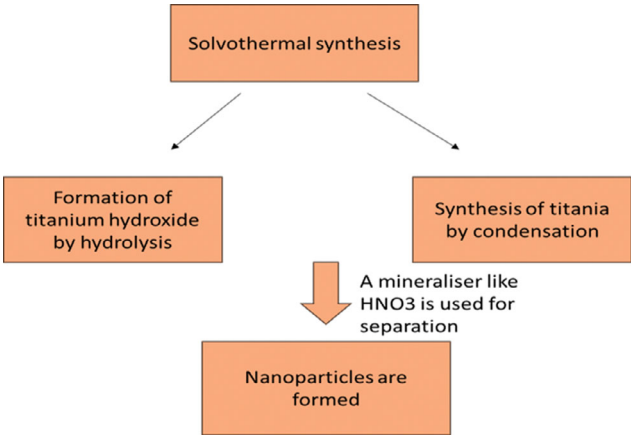

Fig. 5. Solvothermal method.

4. Solvothermal Synthesis

TiO_2 nanoparticles can be synthesized by solvothermal method in which a mixture of solvent technique is used; the result is that size controlled nanoparticles are obtained. A mixture of ethanol and deionized water can be used as a mixed solvent [73]. The two main steps involved in this process include - (A) formation of titanium hydroxide with the help of hydrolysis reaction. (B) the synthesis of titania with the help of condensation reaction. It is difficult to separate the above two reactions which leads to the formation of large sized Titania. However, a mineralizer like HNO_3 is used for separation [74]. Fig. 5 represents the schematic diagram of solvothermal method.

5. Green Synthesis

Green synthesis of TiO_2 nanoparticles can take place by different plant extracts like Moringa olifera leaf extract [75], with the help of papaya leaves [76] (Fig. 6) or by using cinnamon powder extract [77].

6. Microemulsion Method

Surfactants make up micellar structures. The amphiphilic molecules found in surfactants, which typically have a hydrophilic head and a hydrophobic chain, can self-assemble in solution into a wide range of structured structures, including normal and reverse micelles. When the surfactant concentration surpasses the critical micelle concentration, aggregates of surfactant molecules scattered in a liquid colloid are referred to as micelles. Reverse micelles are globular aggregates created when surfactants self-assemble in apolar solvents, whereas regular micelles are created when surfactants self-assemble in water [51,78]. TiO_2 particles were created by Hong et al. [79] utilizing a reverse microemulsion technique using nonionic surfactants with various hydrophilic and hydrophobic groups. Fasolini et al. [80] synthesized TiO_2 nanosphere using Triton X-100 as surfactant and hexanol as co-surfactant. Many more scientists have synthesized TiO_2 based nanomaterial by micro emulsion method.

7. Chemical Vapor Deposition

A technique called chemical vapor deposition (CVD) uses one or more gaseous chemicals or elemental substances containing thin-film components to create thin films by chemical reaction on the surface of substrates. To create precious metal thin films and coatings, CVD is a vital material preparation technique. A variety of processes, including plasma-enhanced chemical vapor deposition (PECVD), plasma-assisted chemical vapour deposition (PACVD), atmospheric-pressure chemical vapor deposition (APCVD), low-pressure chemical vapor deposition (LPCVD), and laser-enhanced chemical vapor deposition, are included in CVD (LECVD) [81]. In the CVD process, a volatile precursor stimulates solid material development at the atomic level in a reaction chamber in the presence of various carrier gases (NH_3, H_2), which is ultimately created on a particular substrate. Substrate temperature and vapor supersaturation are the two elements that cause distinct grain sizes and shapes to develop (Fig. 7) [82].

Metal organic CVD (MOCVD) was used by Pradhan et al. to

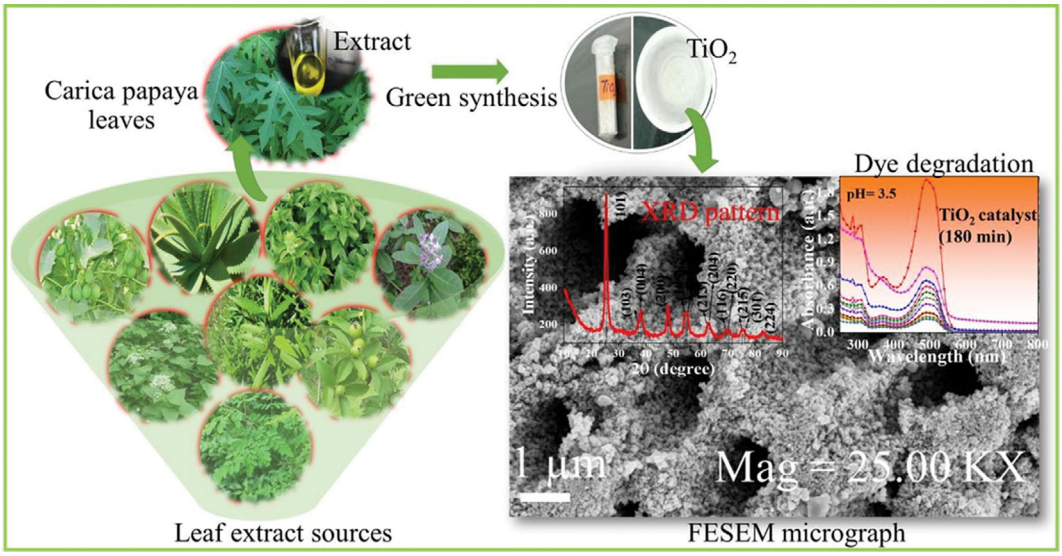

Fig. 6. Green Synthesis of TiO_2 NPs [76].

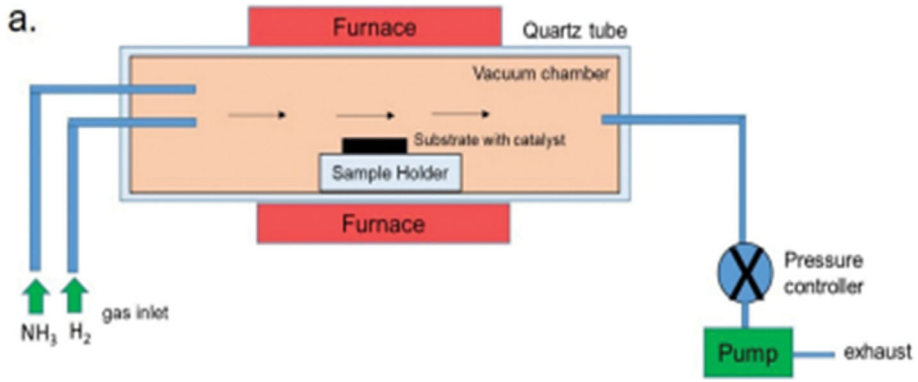

Fig. 7. Schematic Diagram of CVD [82].

create TiO_2 nanorods (50-100 nm) utilizing TTIP as a precursor [82,83]. Using various arc currents, Macwan et al. [82,84] produced pure TiO_2 NPs in a range of sizes. When the current was 80 A, the size ranged from 25 nm to 30 nm, and when the current was 120 A, the size ranged from 30 nm to 42 nm. Zhang et al. created an alternative CVD technique to produce pure anatase-phase TiO_2 films that could withstand and remain stable at high temperatures. The precursor was represented by TTIP, which had a 0.10 mol/L concentration and was dissolved in ethanol. The precursor was then transferred to a reaction chamber, where the substrate underwent post-annealing treatment at high temperatures (600 to 1,100 °C) after being heated at 400 °C using carrier gas and compressed air. The remarkable thermal stability and sheet-like grain structure of the tiny crystalline anatase TiO_2 were evident [82,85].

8. Hydrothermal Method

The hydrothermal synthetic process is often carried out in steel pressure containers, such as autoclaves with Teflon liners, at a controlled temperature and pressure. This temperature can be raised from the water's boiling point to saturation vapor pressure, but the pressure that results also depends on how much additional solution is added [86]. Therefore, numerous researchers have used the hydrothermal approach to create TiO_2 nanoparticles [87-89]. In this regard, Dawson et al. used the hydrothermal approach to create TiO_2 nanoparticles by putting different TiO_2 mixed powder compositions and particle sizes through a hydrothermal reaction in the presence of NaOH [90]. In a comparable experiment, rutile-anatase TiO_2 particles were converted into pure rutile nanotubes using the hydrothermal technique in a NaOH water-ethanol solution, with average diameters smaller than 20 nm [91]. It was observed that the structure and morphology of the products depended on the type of alcohol, as well as the alcohol-water ratio. This was explained by the variation in optoelectronic behaviors of the rutile nanotubes and raw TiO_2. The hydrothermal method was also used to synthesize titanate nanotubes for the degradation of Acid Red 18 [92]. In a different work, titanium (IV) alkoxide was converted into nano-TiO_2 in an acidified water-ethanol solution. TiO_2 nanoparticles dominated by the anatase phase were produced by adding titanium tetraisopropoxide (TTIP) dropwise into the water-ethanol solution at pH 0.7, followed by a four-hour reaction at 240 °C. The as-synthesized nanoparticles were found to range in size from 7 to 25 nm by adjusting the solvent solution and the Ti precursor [93].

9. Microwave Method

The other way to get TiO_2 nanoparticles is by using green technology, by using microwave assisted synthesis; reaction occurs at less time with less use of chemicals and less reaction time [94].

The simplicity, low cost, quicker crystallization time, and greater energy efficiency of the microwave process as compared to traditional heating methods have all contributed to its increased popularity. Since new meta-stable phases may emerge during the preparation of nanocrystalline oxides using the microwave approach, it is a practical method with quick heating to attain the requisite temperature. Using a magnetic stirrer to combine titanium slags and Na_2CO_3, the experimental reaction takes place in this fashion. The residue was collected after three rounds of leaching and washing with water. The residue is then heated to a high temperature of 900 °C for 60 minutes using a microwave with a heating capacity of 1 kilowatt [95].

10. Sonochemical Method

Starting materials for Ti, Zn, and Co are titanium isopropoxide, zinc nitrate hexahydrate, and cobalt nitrate hexahydrate. Zn was kept constant at 1 mol% while Co was adjusted at 1, 2, 3, and 5 mol% in accordance with different concentrations. Zinc nitrate was added after the titanium isopropoxide, which has a concentration of 0.05 M, was dissolved in ethanol and agitated for 20 minutes using a magnetic stirrer. Following the addition of distilled water and Co in various concentrations, the solution was agitated for 15 minutes. After that, 20 ml of NaOH solution (1.875 M) was slowly added to the components while they were exposed to a strong ultrasonic sine wave for 30 minutes at room temperature, until precipitation was observed. The solution was then thoroughly rinsed with distilled water until a pH of 7 was reached, and it was then dried for 12 hours at 120 °C. The product was thus obtained [96].

100 mL of 40% isopropanol solution was poured to a beaker containing 12.7 mL of titanium tetraisopropoxide, and the mixture was agitated for one hour. The samples were then subjected to 0.5 s cycles of sonication lasting 0.5 seconds at 80% of the ultrasound probe-total device's power. After sonication, materials were centrifuged three times, cleaned with methanol, and then transferred to a beaker with a capacity of 250 mL. Following that, the samples underwent a first calcination in a muffler at 200 °C for 1 hour with a heating ramp from 27 to 200 °C at a heating rate of 5 °C/min. They were kept at 200 °C for one hour and cooled to 27 °C at a rate of 5 °C/min. After being kept at 200 °C for an hour, they were cooled at a rate of 5 °C/min from 200 to 27 °C. Following this initial calcination, samples were ground in mortar and pestle to improve particle homogenization. They were then transferred to aluminum boat crucibles and subjected to a second calcination at 600 °C with a 27 to 600 °C heating ramp and a 5 °C/heating rate. Thus product was obtained [97].

STRUCTURAL AND MORPHOLOGICAL STUDY

1. XRD Analysis

Fig. 8 shows XRD analysis of TiO_2 nanoparticles. This XRD pattern was done of TiO_2 nanoparticles that were prepared by glycine assisted gel-combustion method. It was found that pure anatase phase of TiO_2 was observed, which matched with JCPDS card no. 01-084-1286 [98]. The crystallite size can be calculated using Debye-Scherrer's Formula D, [99-101]. The size was found to be 15 nm [102].

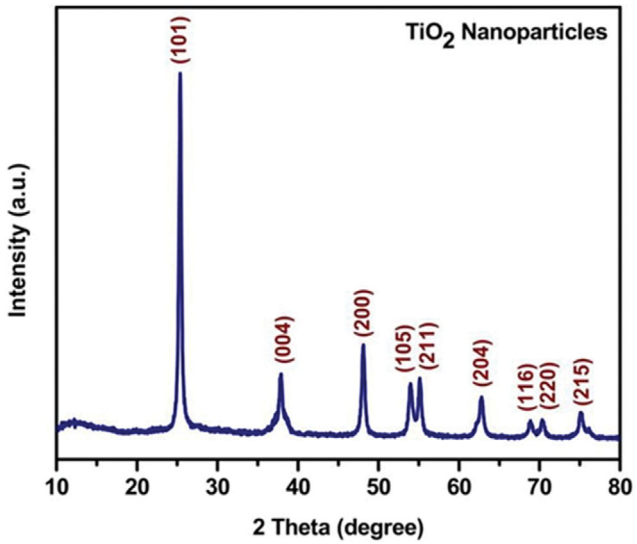

Fig. 8. XRD of TiO_2 NPs [102].

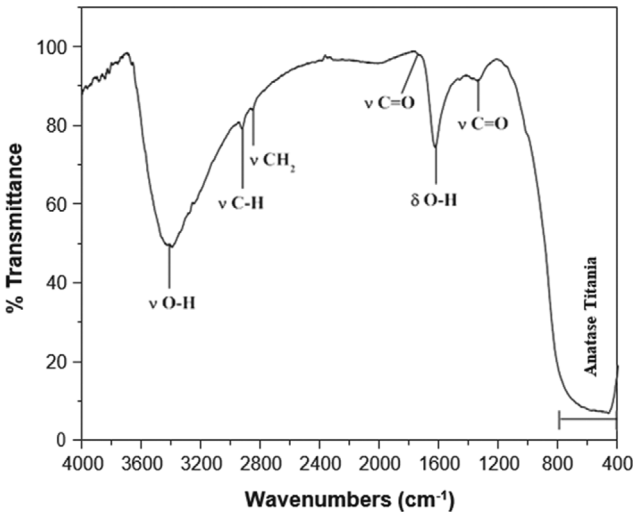

Fig. 9. FTIR Spectrum of Pure Anatase TiO_2 [103]. (With permission © 2013 Elsevier B.V.).

2. Fourier Transform Infrared Spectroscopy

The FTIR of TiO_2 NPs is shown in Fig. 9. This spectrum is of the nanoparticles that were synthesized at 450 °C in air for 4 hours. The end product was white powdered nanoparticles. This FTIR analysis depicts the formation of very pure product and shows the peak of TiO_2. The spectrum showed several peaks: 3,391.72, 2,920.55, 2,849.32, 1,747.95, 1,627.28, 1,342.47, 728.77 and 463.88 cm^{-1} [103]. TiO_2 NPs show hydroxyl groups on the surface. The band is found to be present at 3,391.72 cm^{-1} that report both the symmetric as well as asymmetric stretching of Ti-OH group. There was moisture present in the sample, which was confirmed by peaks present at 3,600 and 3,000 cm^{-1} [103,104]. There are two peaks at 3,391.72 and 1,627.28 cm^{-1} which correlate with surface adsorbed water and

hydroxyl group [103,105]. OH bands are present, showing water adsorbed at surface [103,106]. Ti-O-Ti stretching modes were observed from 1,000 to 4,000 cm^{-1} [103]. The pure peaks of anatase Titania were observed at 463.88 and 728.77 cm^{-1}. Also, there was a broad band describing Ti-O-Ti linkages between 450 and 800 cm^{-1} [103,107]. As per the spectra of TiO_2 there is a peak seen at 463.88

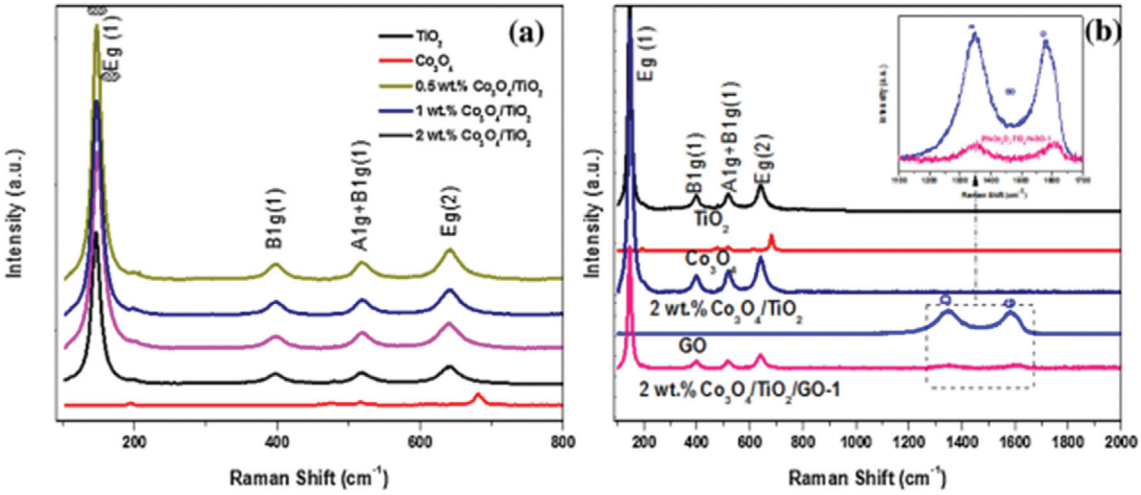

Fig. 10. (a) Raman spectra of (a) Co_3O_4/TiO_2 and (b) As a function of the Co or GO loading, amine functionalized 2 wt% Co_3O_4/TiO_2/GO nanocomposites. For comparison, reference Co_3O_4, anatase, and GO standards are displayed [12].

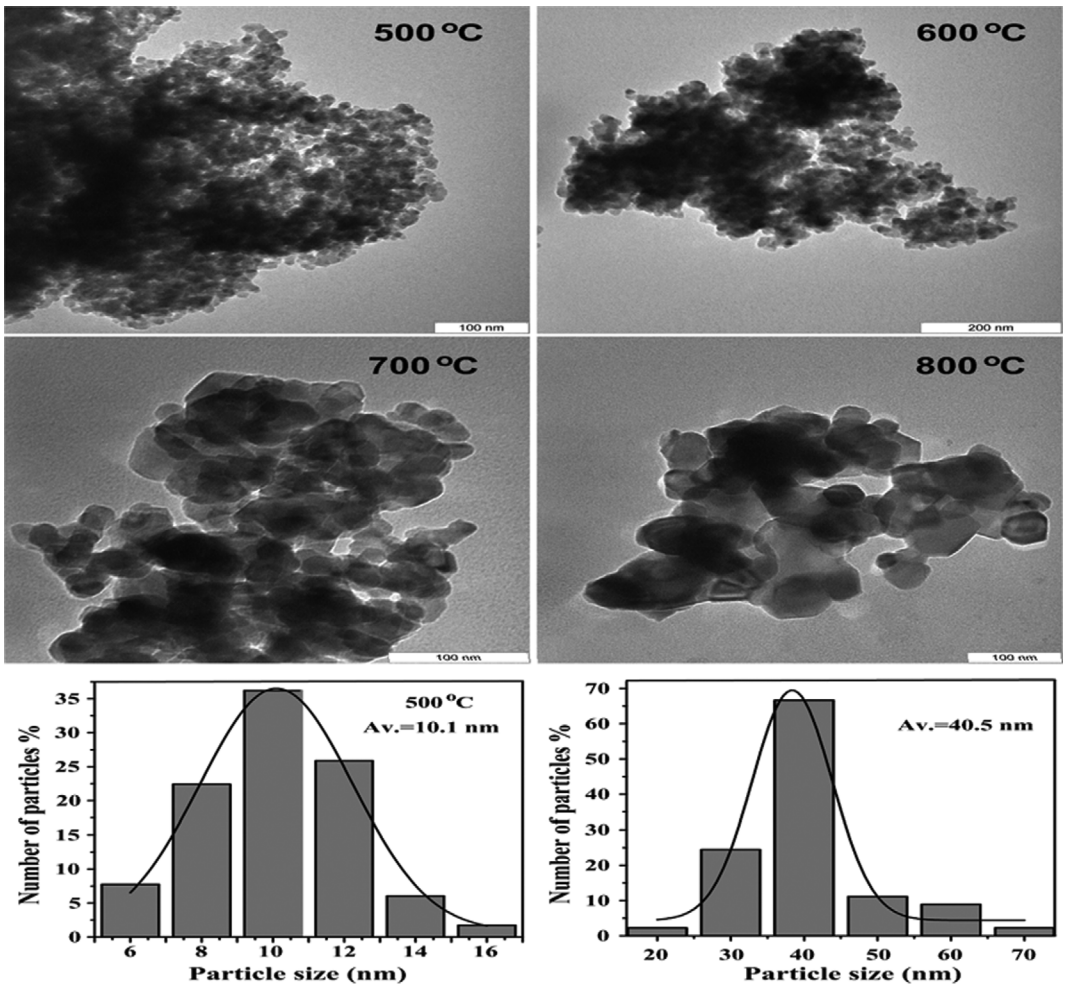

Fig. 11. TEM images for various calcined temperatures and hologram pictures for 500 and 800 °C calcined temperatures [109].

cm^{-1} which is assigned to vibration band of Ti-O bond in TiO_2 [103]. It was found that the prepared product had weak adsorption bands, different organic compounds as well, which were there because the residues were not removed completely by distilled water and ethanol.

This FTIR spectrum shows that Ti-O bond is there, OH is present and peroxo group is absent [108]. Therefore, the FTIR analysis shows the presence of different functional groups in TiO_2.

3. Raman Spectra

Metal oxides and graphene oxide can both be characterized using Raman spectroscopy. The Raman spectra of Co_3O_4/TiO_2 composites as-prepared are shown in Figure. The synthetic Co_3O_4/TiO_2 composites also showed Raman bands at 147, 395, 517, and 638 cm^{-1}, all of which were linked with Eg, B1g, A1g or B1g, and Eg vibrations, showing that titania was present in these materials as anatase. No anatase characteristics differed significantly from pure anatase, showing minimal Co lattice substitution. The poor intensities of Co_3O_4 and the low Co loadings in the composites, however, presumably contributed to the lack of bands attributable to cobalt oxide phases. Two new, faint characteristics indicative of the 'D' and 'G' bands of GO, respectively, appeared at 1,358 cm^{-1} and 1,600 cm^{-1} after GO was added to the Co_3O_4/TiO_2 nanocomposite (Fig. 10) [12].

4. Transmission Electron Microscopy (TEM)

The TEM images (Fig. 11) show the particle size of TiO_2 NPs which were prepared by modified thermal method at lower calcination temperature [109]. At high calcination temperature of 800 °C the particles showed irregular behavior due to agglomeration of particles. TEM images considered 100 particles for each sample. 10.1 and 40.5 nm is the average particle size at 500 and 800 °C [109]. The end result was that with the increase in temperature the particle size also increased, because many particles interacted and fused with each other to form large particles [110].

5. Scanning Electron Microscopy (SEM) and Energy X-Ray Dispersive Spectroscopy (EDS) Analysis

Here the TiO_2 nanoparticles were synthesized by electrochemical method and the SEM graph was obtained at 10 mA/cm^2 and 14 mA/cm^2 which depicted agglomeration of particles and irregularity, which may have been due to partial solubility of surfactant in solvent during the experiment. The TiO_2 NPs synthesized were

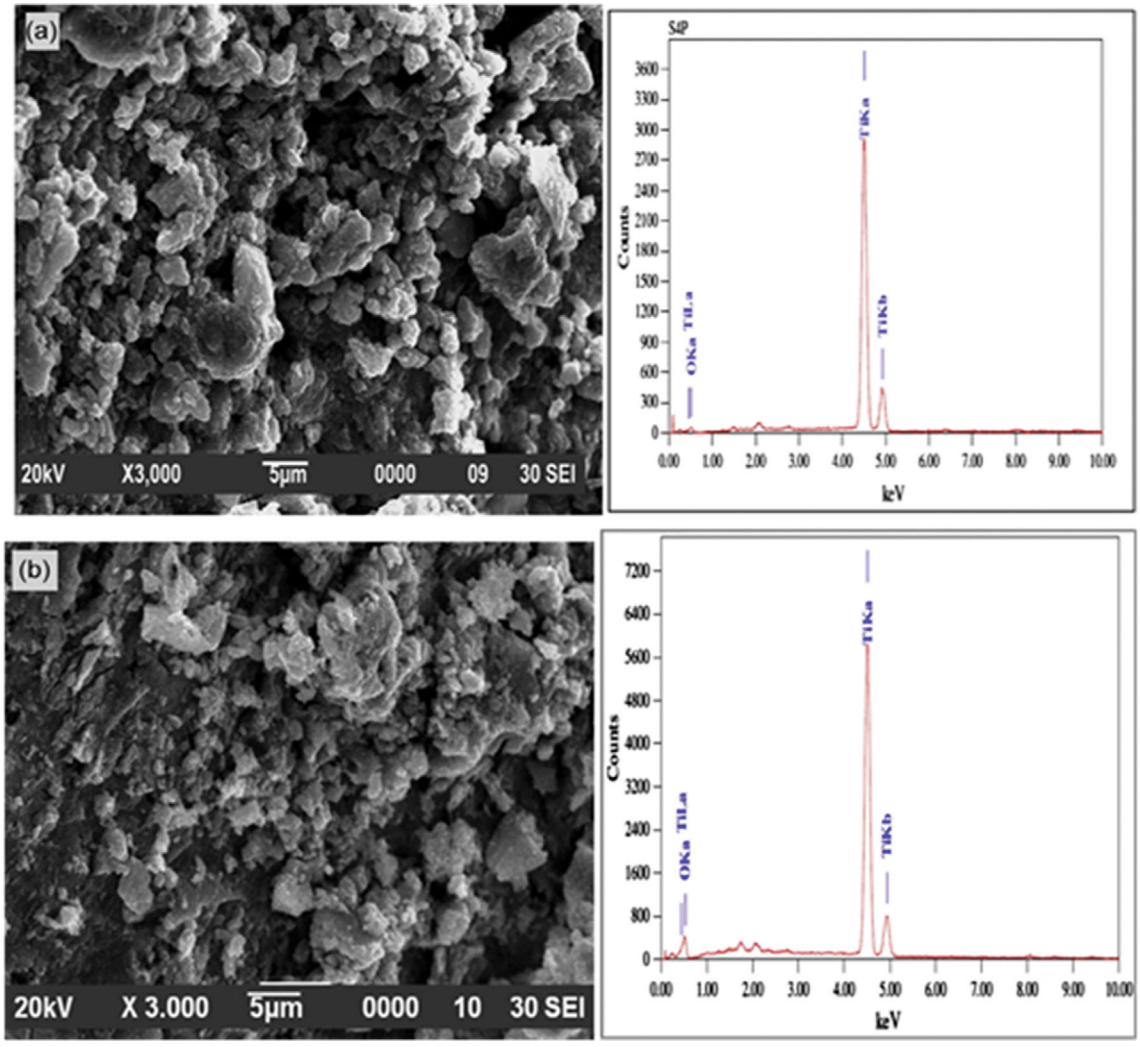

Fig. 12. TiO_2 SEM Images (a) with respect to 10 mA/cm^2 and (b) with respect to 14 mA/cm^2 with EDS spectra, respectively [68].

then examined by EDS, which is shown in Fig. 12. EDS spectra showed that pure TiO_2 was formed as only the peaks of Ti and O were observed indicating the removal of capping agent [68].

STRUCTURE AND ACTIVITY OF TITANIUM OXIDE AS A PHOTOCATALYST

The natural titanium oxide crystal structure can be classified as anatase, rutile, and brookite. There is no difference in the chemical formula for titania (TiO_2) between these three types, but there is a difference in the crystal structure. By absorbing light with an energy level above the band gap, titanium oxide creates positive holes in the valence band by causing electrons to jump to the conduction band. The band gap values for rutile and anatase are each 3.0 eV, but only ultraviolet rays can pass through them. Rutile, on the other hand, absorbs rays that are closer to visible light rays. The rutile type is more suited for use as a photocatalyst because it can absorb a wider range of light. Anatase, however, shows higher photocatalytic activity in reality. Due to their different energy structures, the two types differ in this regard. Valence bands are deep in both types, resulting in positive holes with sufficient oxidative power. Both types are relatively weak in terms of reducing power due to the conduction band being located near hydrogen's oxidation-reduction potential (Fig. 13) [111].

MECHANISM OF TITANIUM-OXIDE PHOTOCATALYTIC REACTIONS [111,112]

Although the valence band and conduction band creation processes in a compound semiconductor are intricate, the underlying principles are straightforward. While titanium's 3d orbital generates the conduction band in titanium oxide, oxygen's 2p orbital creates the valence band. Electrons in the valence band of a semiconductor with a wide band gap are unable to move into the conduction band (Fig. 14).

However, electrons in the valence band can be excited to the

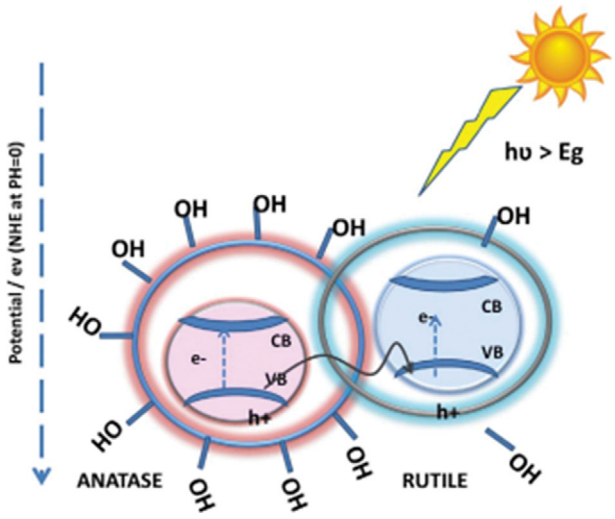

Fig. 13. Anatase and rutile energy band diagrams [111]. (with Permission © 2017 Elsevier Ltd.).

conduction band if energy is provided outside. As a result, the quantity of electrons stimulated in the valence band is equal to the quantity of electron holes (holes created as a result of electrons migrating up to the conduction band). The transfer of electrons from a bonding orbital to an antibonding orbital is analogous to this. We might also state that a semiconductor's photoexcited state is typically unstable and prone to disintegration. Even after being photoexcited, titanium oxide maintains its stability. This is just one of the factors that make titanium oxide a great photocatalyst.

PHOTOCATALYST AND PHOTOCATALYTIC EFFICIENCIES (TABLE 2)

1. UV-visible Spectroscopy of TiO_2 Nanoparticles

The optical property of TiO_2 nanoparticles can be obtained with the help of UV-Vis spectroscopy. The UV-Vis absorption spectrum

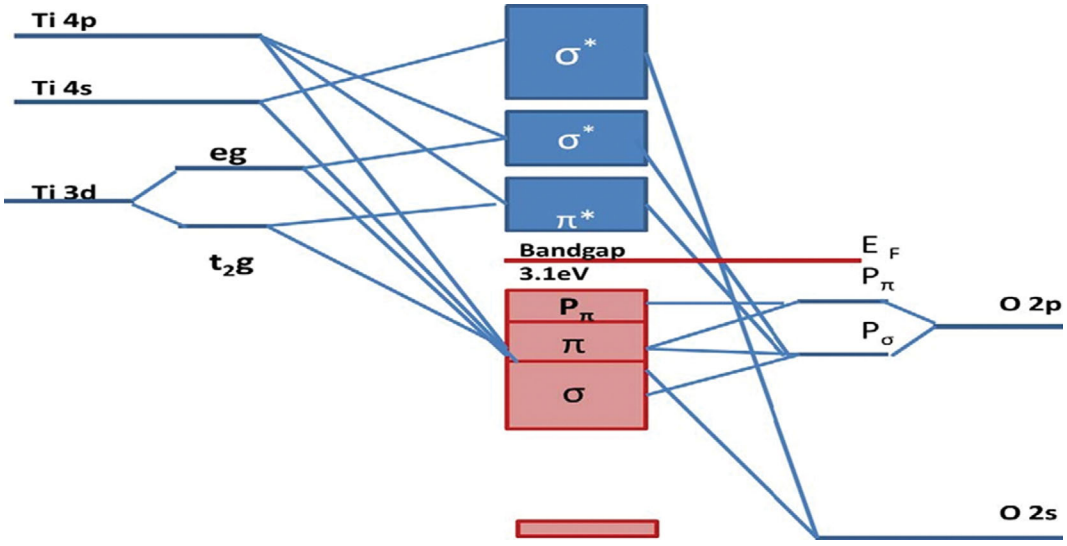

Fig. 14. Molecular Orbital Diagram of TiO_2 [111]. (Reproduced with permission © 2017 Elsevier Ltd.).

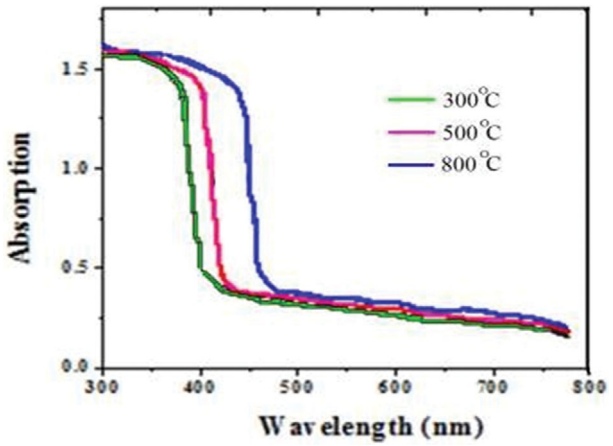

Fig. 15. UV-vis absorption spectra of TiO_2 NPs at different calcined temperatures [113]. (With permission © 2016 Elsevier GmbH).

of TiO_2 nanoparticles is shown in Fig. 15. The band gap (Eg) is calculated by the following equation Eg- where λ is wavelength in nm.

Table 1. Band gap values at different calcined temperatures [113] (with permission © 2016 Elsevier GmbH)

Temperature (°C)	Band Gap (Eg In Ev)
300	3.02
500	2.95
800	2.75

Fig. 14 depicts that the absorption spectrum calcined at 300 °C at wavelength 410 nm shows a band gap of 3.02 eV as pure anatase phase was present. The TiO_2 nanoparticles calcined at 500 and 800 °C, respectively, showed absorption at 420 nm and 450 nm and depicted large particle size. There is a shift in spectrum from UV to Visible range at high calcined temperature and thus there is changes band gap as well (Table 1) [113].

Qutub et al. [152] studied degradation of acid blue dye using CdS/TiO_2 nanocomposite under visible light and photodegradation was found to be 84%. Castro et al. [153] studied photocatalytic degradation of Orange-122 dye using Zn/TiO_2 catalyst under UV radiation at 400 °C calcined temperature and the best result of

Table 2. Photocatalytic degradation efficiencies of different textile dye with respect to TiO_2 based nanomaterials

Photocatalyst	Dyes	Source	Degradation efficiency %	Time taken (minute)	Ref.
Pure TiO_2 film	Methylene blue	UV	62.1	60	[114]
Zn (3 mol%) doped with TiO_2	Methylene blue Methyl orange	UV	97.3 95.6	60	[114]
Pure TiO_2 film	Methylene orange	UV	51.6	60	[114]
TiO_2 nanoparticle supported with ceramic	Methylene blue	UV	65	60	[115]
TiO_2	Congo red	UV	66.99	30	[116]
TiO_2	Congo red	Solar	64.72	30	[116]
TiO_2	Alizarin yellow Acid orange Crystal violet	Solar	65 66 82	90	[117]
4% wt CO-Cu_2O/TiO_2	Reactive blue 49	UV	76	80	[118]
TiO_2 anatase	Reactive blue 49 Reactive yellow 160	UV	28.1 33.8	80	[118]
Fe-TiO_2/rGO	Rhodamine B	Solar	91	120	[119]
Pure TiO_2	Rhodamine 6G	Solar	42	60	[120]
Graphene-TiO_2	Rhodamine 6G	Solar	98	60	[120]
TiO_2-p25	Trypan blue	Solar	81	30	[121]
Nano-TiO_2	Trypan blue	Solar	100	30	[121]
TiO_2	Victoria blue R	UV	98	30	[122]
GO/TiO_2	Methyl orange	UV	96	80	[123,124]
r-GO/TiO_2	Rhodamine B	Solar	99.8	120	[123,124]
r-GO/Fe_3O_4-TiO_2	Malachite green	Visible	99	55	[123,124]
Nb-TiO_2/r-GO	Rhodamine B	Visible	98	90	[123,127]
TiO_2/Nb_2O_5/rGO	Methyl orange Methylene blue	Visible	93 97	240	[128,129]

Table 2. Continued

Photocatalyst	Dyes	Source	Degradation efficiency %	Time taken (minute)	Ref.
TiO_2/rGO	Methyl orange Methylene blue	Visible	78 82	240	[128,129]
TiO_2/r-GO (5%)	Methylene blue Rhodamine B	Solar	99.6 99.9	120	[130]
TiO_2/r-GO (15%)	Methylene blue Rhodamine B	Solar	98.1 99.8	120	[130]
F-TiO_2(B)	Malachite green	Visible	54.26	120	[131]
F-TiO_2(B)/MWCNT	Malachite green	Visible	88.89	120	[132]
F-TiO_2(B)/SWCNT	Malachite green	Visible	91.83	120	[131]
TiO_2	Malachite green	UV	99.9	60	[131,132]
TiO_2/MWCNT	Methyl orange	Visible	94	120	[131,133]
ZnO-TiO_2 film	Methylene blue	Germicidal lamp	44	120	[134,135]
ZnO-TiO_2 rod sphere on film	Methyl orange	Mercury lamp	39	120	[135]
C(2%)/TiO_2	Methylene blue	Sun light	-	120	[136]
0.7-SnO_2/TiO_2 NTAs	Methylene blue Rhodamine B	Xe Lamp	94.71 80.58	90	[137]
$Bi_2Sn_2O_7$/TiO_2 NTAs	Methyl orange Rhodamine B Methylene blue	Solar	63.76 77.34 100	-	[138]
PANI-TiO_2/rGO	Rhodamine B	Xe Lamp	90.5%	30	[139]
CdS/TiO_2	Acid blue-29	Visible light	84	90	[140]
PANI/TiO_2/cotton	Rhodamine B	Visible	87.67	180	[139,141]
PANI/$Ti_{0.91}O_2$	Rhodamine B	Visible	81.7	360	[139,142]
TiO_2/PANI	Rhodamine B	UV	80	180	[139,143]
Au-PANI@TiO_2	Rhodamine B	Visible	90	140	[139,144]
Ag/Ag_3VO_4/TiO_2	Rhodamine B	Visible	97.3	45	[145]
PVA aerogel/TiO_2/MoS_2/Au composite	Rhodamine B	Visible	86	240	[146]
Fe-TiO_2/AC	Cibacron Yellow F-4G	Visible	100	120	[2]
Co-TiO_2/AC	Cibacron Yellow F-4G	Visible	100	120	[2]
Co_3O_4/TiO_2/GO	Congo red	Xe 300 W	91	90	[12]
C-TiO_2	Reactive blue-19 Reactive red-76	Visible light	100	60	[147]
S-TiO_2	Reactive blue-19 Reactive red-76	Visible light	100	60	[147]
C,S-TiO_2	Reactive blue-19 Reactive red-76	Visible light	100	60	[147]
TiO_2-rGO	Rhodamine B	Visible	81	320	[139,148]
45% SiO_2/TiO_2 composite	Methylene blue	UV	91.20	50	[149]
Mesoporous-TiO_2	Methylene blue	UV	99.27	50	[149]
Ag_3PO_4/TiO_2/SiO_2	Methylene blue	150-W Xenon lamp	99	20	[150]
PANI/TiO_2	Methylene blue	Visible	96	240	[151]

Abbreviations used: r-GO- reduced graphene oxide, F- fluorine, B- bronze, MWCNT- multiwalled carbon nano tubes, SWCNT- single walled carbon nano tubes, NTAs – Nanotube arrays, AC- Activated Carbon, PANI-polyaniline

discoloration was 99.76% after a reaction time of 2 hours. Chhtu Ram et al. [154] studied photocatalytic degradation of Procion Yellow using TiO_2 under UV light and found 83.6% degradation of dye at pH 7.8 after time interval of 3.5 hours. Redha et al. [155] studied the photocatalytic degradation of azo dye, i.e., Novacron Red C-2BL under UV light using TiO_2 film and found the best result of 98% degradation at pH 7 after a reaction time of 100 min. Noaman et al. [156] studied the photo degradation of Reactive Red 120 using TiO_2 catalyst under both UV and solar UV radiation and found degradation to be 67.37% and 99.09%, respectively.

Almhana et al. [157] tried to remove Acid Blue -113 dye from wastewater under UV radiation using ZnS/TiO_2 nanocomposite at pH 6.2 and found photocatalytic degradation efficiency to be 97%. Kukarni et al. [158] studied the photodegradation of Navy Blue HE2R dye using Degussa P-25 TiO_2 using UV light and found degradation efficiency to be 92.91% after a time of 3 hours. Trivedi et al. [159] studied solar light induced photocatalytic degradation of Coralene Dark Red 2B dye under UV light with the help of TiO_2 catalyst and found degradation efficiency to be 98% which was achieved at time 120 min.

Rezig et al. [160] studied the photodegradation of Vat Green 03 textile dye using Ferrihydrite - modified process with TiO_2 nanocatalyst, and the result obtained was 97% degradation efficiency at pH 4. Stoyanova et al. [161] performed an experiment on photocatalytic degradation of a single and binary mixture of two dyes. Reactive Black 5 and Congo Red. using lanthanum modified TiO_2 nanocatalyst, and the degradation efficiency was found to be 88% and 67%, respectively, after 60 minutes of UV irradiation. Giwa et al. [162] used Reactive Yellow 81 and Reactive Violet 1 to check the photocatalytic degradation efficiency of these two dyes using TiO_2-P25 photocatalyst under sunlight and obtained 92% and 85% degradation efficiency after 20 minutes. Yang et al. synthesized Au-modified nanosheet-branched TiO_2 hollow spheres with different concentrations of Au (1%, 5%, and 8%) and studied the photodegradation of R6G. The degradation rate of R6G was found to be for 1% Au/Tio2, 5% Au/Tio2 and 8% Au/Tio2 are 96.4 %, 96.9% and 96.5%, respectively [163].

REACTION MECHANISM

A semiconductor material's VB and CB are photo-excited and photo-absorbed as part of the general mechanism of photocatalysis. Researchers have postulated a number of methods for the production of electron-holes, their transport across the valence, conduction, and forbidden energy bands, as well as their recombination [164].

Fig. 16(a) shows orange II and rhodamine B and TiO_2 band gap energies compared to NHE reference electrodes in valence and conduction bands. There are 2.37 eV [165,166] energy bands for rhodamine B, 2.03 eV [165,166] energy bands for orange II and 3.2 eV [165,166] energy bands for TiO_2. It is possible to absorb visible light through orange II and rhodamine B due to their narrow band gap energies. In contrast, due to the much higher potential of OII and RhB lattice unoccupied molecular orbitals (LUMOs) than TiO_2 conduction band (CB), [166,167] electrons can be transferred from LUMOs to CBs. As reported in [168], $O_2/{}^{\bullet}O_2^-$ redox

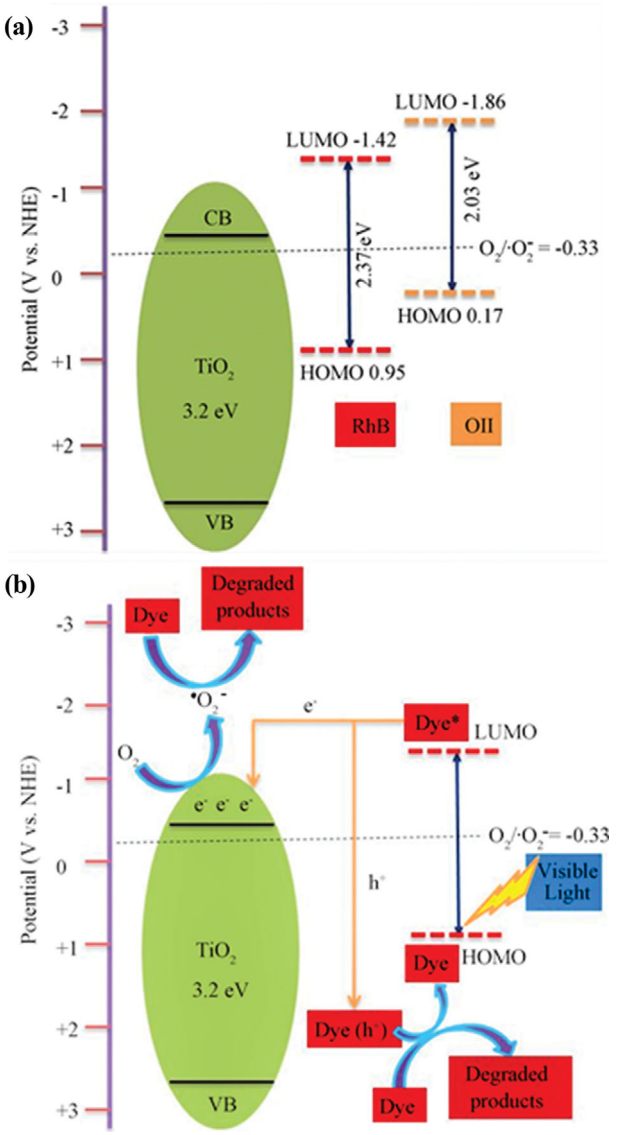

Fig. 16. Under visible light irradiation, the reaction of superoxide radicals ($^{\bullet}O_2^-$) and holes (h^+) with TiO_2 is shown by a schematic (a) and (b) of the mechanisms of self-sensitized TiO_2 reaction [165].

potential is only- 0.33 V compared with NHE, which makes it less negative than TiO_2 conduction band potential [169]. Fig. 16(b) shows a dye-sensitized mechanism under visible light irradiation (b). When exposed to visible light, a dye absorbs it and converts it into an electron and a hole in its valence and conduction bands (LUMO and HOMO), respectively [170]. Then, the electron in the LUMO moves to the CB of the TiO_2. To create O_2, the adsorbed molecular oxygen on the catalyst takes one electron from the CB of TiO_2. Adsorbed dye reacts with the oxidant ($^{\bullet}O_2^-$) radical to destroy it. The HOMO's holes react with the adsorbed OH^- species to create an OH radical.

Here is a description of a potential degradation reaction process.

$$\text{Dye} + \text{visible light} \rightarrow \text{dye}(e^- + h^+) \quad (1)$$

$$\text{Adsorbed dye}(e^- + h^+) + TiO_2 \rightarrow TiO_2(e) + \text{dye}(h^+) \quad (2)$$

$$TiO_2(e) + \text{adsorbed } O_2 \rightarrow TiO_2 + {}^{\bullet}O_2^- \quad (3)$$

$$\text{Adsorbed dye} + \text{dye}(h^+) \rightarrow \text{degradation} \quad (4)$$

$${}^{\bullet}O_2^- + \text{adsorbed dye} \rightarrow \text{degraded or mineralized products} \quad (5)$$

CONCLUSION AND FUTURE SCOPE

This review concentrated on a thorough investigation of the fundamental properties of TiO_2 nanoparticles and nanocomposite made of TiO_2. The best visible-light-driven photocatalyst for degrading a variety of dyes is thought to be titania. In order to address the environmental pollution issues brought on by industrial effluents or other pollutants, much research has been done that highlights the significance of non-metals/metal-doped titania in comparison to the undoped TiO_2 for their better photocatalytic dye degradation of various anionic and cationic dyes. The impact of various factors, including pH, dye concentration, photocatalyst size and structure, pollutants concentration and type, photocatalyst surface area, the effect of light intensity along with its irradiation time, catalyst loading, variation in temperature, and the impact of doping with optimization, has a strong correlation with pollutant degradation rate, which is also covered in this review. The development of effective synthesis techniques can further enhance the photocatalytic performance of titania-based materials.

However, all potential industrial uses are affected by the photocatalytic materials' progressive deactivation. The photocatalytic materials would need to be periodically renewed, which would raise the overall cost. Cost would therefore undoubtedly continue to be a key concern for commercialization. So, to overcome this challenge, in-depth study will be required to create affordable reactors as well as photocatalytic materials. The simultaneous, concerted, and substantial research progress required to accomplish these objectives is essential for the use of this technology in the real world.

CONFLICT OF INTEREST STATEMENT

There is no conflict of interest between authors.

DATA AVAILABILITY STATEMENT

Data sharing not applicable to this article as no datasets were generated.

REFERENCES

1. P. Akhter, A. Arshad, A. Saleem and M. Hussain, *Catalysts*, **12**, 1331 (2022).
2. R. M. Garcia, R. Carleer, M. A. Pérez, J. P. Torres, Y. Gu, P. Samyn and J. Yperman, *Catalysts*, **11**, 1137 (2021).
3. S. Rajagopal, B. Paramasivam and K. Muniyasamy, *Sep. Purif. Technol.*, **252**, 117444 (2020).
4. R. Giovannetti, R. Giovannetti, C. A. D'Amato, M. Zannotti, E. Rommozzi, R. Gunnella, M. Minicucci and A. Di Cicco, *Sci. Rep.*, **5**, 17801 (2015).
5. B. R. Babu, A. K. Parande, S. Raghu and T. P. Kumar, *J. Cotton Sci.*, **11**, 141 (2007).
6. A. Mills and S. Le Hunte, *J. Photochem. Photobiol. A.*, **108**, 1 (1997).
7. A. Fujishima, T. N. Rao and D. A. Tryk, *J. Photochem.*, **1**, 1 (2000).
8. C. Thambiliyagodage and S.Mirihana, *J. Sol Gel Sci. Technol.*, **99**, 109 (2021).
9. I. T. Peternel, N. Koprivanac, A. M. L. Božić and H. M. Kušić, *J. Hazard. Mater.*, **148**, 477 (2007).
10. W. Przystaś, E. Zabłocka-Godlewska and E. Grabińska-Sota, *Water Air Soil Pollut.*, **223**, 1581 (2012).
11. M. M. Mahlambi, C. J. Ngila and B. B. Mamba, *J. Nanomater.*, **2015**, 1 (2015).
12. W.-K. Jo, S. Kumar, M. A. Isaacs, A. F. Lee and S. Karthikeyan, *Appl. Catal. B.*, **201**, 159 (2017).
13. M. Rani, U. Shanker and V. Jassal, *J. Environ. Manag.*, **190**, 208 (2017).
14. R. Gusain, K. Gupta, P. Joshi and O. P. Khatri, *Adv. Colloid Interface Sci.*, **272**, 102009 (2019).
15. G. Crini and E. Lichtfouse, *Environ. Chem. Lett.*, **17**, 145 (2019).
16. C. G. Joseph, G. Li Puma, A. Bono and D. Krishnaiah, *Ultrason. Sonochem.*, **16**, 583 (2009).
17. D. Zhu and Q. Zhou, *Environ. Nanotechnol. Monit. Manag.*, **12**, 100255 (2019).
18. T. Singh, N. Srivastava, P. K. Mishra, A. K. Bhatiya and N. L. Singh, *Mater. Sci. Forum.*, **855**, 20 (2016).
19. C. B. Anucha, I. Altin, E. Bacaksiz and V. N. Stathopoulos, *Chem. Eng. J. Adv.*, **10**, 100262 (2022).
20. J. Schneider, M. Matsuoka, M. Takeuchi, J. Zhang, Y. U. Horiuchi, M. Anpo and D. W. Bahnemann, *Chem. Rev.*, **114**, 9919 (2014).
21. M. Shahrezaei, A. A. Babaluo, S. Habibzadeh and M. Haghighi, *Eur. J. Inorg. Chem.*, **3**, 694 (2017).
22. M. R. Hoffmann, S. T. Martin, W. Choi and D. W. Bahnemann, *Chem. Rev.*, **95**, 69 (1995).
23. S. Kment, F. Riboni, S. Pausova, L. Wang, L. Wang, H. Han, Z. Hubicka, J. Krrysa, P. Schmuki and R. Zboril, *Chem. Soc. Rev.*, **46**, 3716 (2017).
24. M. Bernareggi, M. Dozzi, L. Bettini, A. Ferretti, G. Chiarello and E. Selli, *Catalysts*, **7**, 301 (2017).
25. T. Sakata, *J. Photochem.*, **29**, 205 (1985).
26. H. Kisch, *Angew. Chem. Int. Ed. Engl.*, **52**, 812 (2013).
27. A. Fujishima, T. N. Rao and D. A. Tryk, *J. Photochem. Photobiol. C.*, **1**, 1 (2000).
28. T. L. Thompson and J. T. Yates, *Chem. Rev.*, **106**, 4428 (2006).
29. M. Manzoor, A. Rafiq, M. Ikram, M. Nafees and S. Ali, *Int. Nano Lett.*, **8**, 1 (2018).
30. R. D. C. Soltani, M. Mashayekhi, M. Naderi, G. Boczkaj, S. Jorfi and M. Safari, *Ultrason. Sonochem.*, **55**, 117 (2019).
31. H. Lachheb, E. Puzenat, A. Houas, M. Ksibi, E. Elaloui, C. Guillard and J. M. Herrmann, *Appl. Catal. B.*, **39**, 75 (2002).
32. A. Fernandes, P. Makoś, Z. Wang and Boczkaj, *Chem. Eng. J.*, **391**, 123488 (2020).
33. W. Buraso, V. Lachom, P. Siriya and P. Laokul, *Mater. Res. Express.*, **5**, 115003 (2018).
34. S. Çeşmeli and C. B. Biray Avci, *J. Drug Target.*, **27**, 762 (2019).
35. M. D. Newman, M. Stotland and J. I. Ellis, *J. Am. Acad. Dermatol.*, **61**, 685 (2009).
36. L. M. Anaya-Esparza, Z. Villagrán-de la Mora, J. M. Ruvalcaba-Gómez, R. Romero-Toledo, T. Sandoval-Contreras, S. Aguilera-

Aguirre, E. Montalvo-González and A. Pérez-Larios, *Processes*, **8**, 1395 (2020).
37. N. Zhang, S. Qiao and V. K. Gupta, *Opt. Mater.*, **120**, 111452 (2021).
38. Y. Liu, Z. Xu, S. Zhu, A. Fakhri and V. K. Gupta, *J. Photochem. Photobiol. A.*, **422**, 113522 (2022).
39. A. Bahadoran, M. Najafizadeh, Q. Liu, J. R. De Lile, D. Zhang, S. Masudy-Panah, S. Ramakrishna, A. Fakhri and V. K. Gupta, *Surf. Interfaces*, **26**, 101279 (2021).
40. S. Xiao, A. Fakhri and B. J. Janani, *Surf. Interfaces*, **27**, 101490 (2021).
41. A. Bahadoran, Q. Liu, B. Liu, J. Gu, D. Zhang, A. Fakhri and V. Kumar Gupta, *Spectrochim. Acta A Mol. Biomol. Spectrosc.*, **253**, 119592 (2021).
42. Y. Mao, J. Qiu, P. Zhang, Z. Fei, C. Bian, B. J. Janani and A. Fakhri, *J. Photochem. Photobiol. A.*, **426**, 113756 (2022).
43. W. Long, M. U. Hamza, M. N. Abdul-Fattah, A. M. Rheima, Y. M. Ahmed, F. S. Fahim, U. S. Altimari, A. K. O. Aldulaim, B. J. Janani and A. Fakhri, *Colloids Surf. A Physicochem. Eng. Aspects*, **650**, 129468 (2022).
44. A. Bahadoran, N. B. Baghbadorani, J. R. De Lile, S. Masudy-Panah, B. Sadeghi, J. Li, S. Ramakrishna, Q. Liu, B. J. Janani and A. Fakhri, *J. Photochem. Photobiol. B.*, **228**, 112393 (2022).
45. Y. Cai, F. Yang, L. Wu, Y. Shu, G. Qu, A. Fakhri and V. Kumar Gupta, *Mater. Chem. Phys.*, **258**, 123919 (2021).
46. I. Mahboob, I. Shafiq, S. Shafique, P. Akhter, M. Munir, M. Saeed, M. S. Nazir, Um-e-S. Amjad, F. Jamil, N. Ahmad, Y-K. Park and M. Hussain, *Chemosphere*, **311**, 137180 (2023).
47. M. Shabir, M. Yasin, M. Hussain, I. Shafiq, P. Akhter, A. S. Nizami, B. H. Jeon and Y. K. Park, *J. Ind. Eng. Chem.*, **112**, 1 (2022).
48. K. Azam, N. Shezad, I. Shafiq, P. Akhter, F. Akhtar, F. Jamil, S. Shafique, Y.-K. Park and M. Hussain, *Chemosphere*, **306**, 135566 (2022).
49. N. Shehzad, M. Tahir, K. Johari, T. Murugesan and M. Hussain, *J. CO_2 Util.*, **26**, 98 (2018).
50. M. Sharon, F. Modi and M. Sharon, *AIMS Mater. Sci.*, **3**, 1236 (2016).
51. S. Lee, I.-S. Cho, J. H. Lee, D. H. Kim, D. W. Kim, J. Y. Kim, H. Shin, J.-K. Lee, H. S. Jung, N.-G. Park, K. Kim, M. J. Ko and K. S. Hong, *Chem. Mater.*, **22**, 1958 (2010).
52. R. S. Dubey, K. V. Krishnamurthy and S. Singh, *Results Phys.*, 102390 (2019).
53. M. M. Ahmad, S. Mushtaq, H. S. Al Qahtani, A. Sedky and M. W. Alam, *Crystals*, **11**, 1456 (2021).
54. M. Hussain, R. Ceccarelli, D. L. Marchisio, D. Fino, N. Russo and F. Geobaldo, *Chem. Eng. J.*, **157**, 45 (2010).
55. M. Hussain, N. Russo and G. Saracco, *Chem. Eng. J.*, **166**, 138 (2011).
56. R. Rashid, I. Shafiq, M. J. Iqbal, M. Shabir, P. Akhter, M. H. Hamayun, A. Ahmed and M. Hussain, *J. Environ. Chem. Eng.*, **9**, 105480 (2021).
57. S. Kumar, S. Jain and B. Y. Lamba, *Int. J. Environ. Anal. Chem.*, 1 (2021).
58. G. K. Upadhyay, J. K. Rajput, T. K. Pathak, V. Kumar and L. P. Purohit, *Vacuum*, **160**, 154 (2019).
59. R. S. Sabry, Y. K. Al-Haidarie and M. A. Kudhier, *J. Sol Gel Sci. Technol.*, **78**, 299 (2016).
60. M. M. Ali, M. J. Haque, M. H. Kabir, M. A. Kaiyum and M. S. Rahman, *Results Mater.*, **11**, 100199 (2021).
61. S. Cho, J.-W. Jang, K.-H. Lee and J. S. Lee, *APL Mater.*, **2**, 010703 (2014).
62. A. T. Güntner, N. J. Pineau, D. Chie, F. Krumeich and S. E. Pratsinis, *J. Mater. Chem. B.*, **4**, 5358 (2016).
63. A. Eslami, M. M. Amini, A. R. Yazdanbakhsh, A. Mohseni-Bandpei, A. A. Safari and A. Asadi, *J. Chem. Technol. Biotechnol.*, **91**, 2693 (2016).
64. E. T. Helmy, A. El Nemr, M. Mousa, E. Arafa and S. Eldafrawy, *J. Water Environ. Nanotechnol.*, **3**, 116 (2018).
65. D. V. Aware and S. S. Jadhav, *Appl. Nanosci.*, **6**, 965 (2016).
66. K. Meesombad, N. Sato, S. Pitiphattharabun, G. Panomsuwan, R. Techapiesancharoenkij, K. Surawathanawises, C. Wongchoosuk, S. Boonsalee, J. H. Pee and O. Jongprateep, *Ceram. Int.*, **47**, 21099 (2021).
67. P. Szołdra, M. Frąc and W. Pichór, *Powder Technol.*, **387**, 261 (2021).
68. P. Anandgaonker, G. Kulkarni, S. Gaikwad and A. Rajbhoj, *Arab. J. Chem.*, **12**, 1815 (2019).
69. I. Bezares, A. del Campo, P. Herrasti and A. Muñoz-Bonilla, *Phys. Chem. Chem. Phys.*, **17**, 29319 (2015).
70. W. Buraso, V. Lachom, P. Siriya and P. Laokul, *Mater. Res. Express.*, **5**, 115003 (2018).
71. S. Pang, J. G. Huang, Y. Su, B. Geng, S. Y. Lei, Y. T. Huang, C. Lyu and X. J. Liu, *Photochem. Photobiol.*, **92**, 651 (2016).
72. J. Deng, M. Wang, Junfei Fang, X. Song, Z. Yang and Z. Yuan, *J. Alloys Compd.*, **791**, 371 (2019).
73. V. M. Ramakrishnan, M. Natarajan, A. Santhanam, V. Asokan and D. Velauthapillai, *Mater. Res. Bull.*, **97**, 351 (2018).
74. J. Li, Q. Wu and J. Wu, *Handbook of nanoparticles*, Springer International Publishing, Switzerland (2016).
75. V. Patidar and P. Jain, *Int. Res. J. Eng. Technol.*, **4**, 1 (2017).
76. H. Kaur, S. Kaur, J. Singh, M. Rawat and S. Kumar, *Mater. Res. Express.*, **6**, 095034 (2019).
77. G. Nabi, W. Raza and M. B. Tahir, *J. Inorg. Organomet. Polym. Mater.*, **30**, 1425 (2020).
78. D. Zhang, L. Qi, J. Ma and H. Cheng, *J. Mater. Chem.*, **12**, 3677 (2002).
79. M. S. Lee, S. S. Park, G. Lee, C. Ju and S. Hong, *Cat. Today*, **101**, 283 (2005).
80. A. Fasolini, E. Lombardi, T. Tabanelli and F. Basile, *Nanomaterials (Basel)*, **11**, 1175 (2021).
81. L. Xia, *Bioceramics*, **5** (2021).
82. V. D. Matteis, A. Cannavale and U. Ayr, *Appl. Sci.*, **10**, 8896 (2020).
83. S. K. Pradhan, P. J. Reucroft, F. Yang and A. Dozier, *J. Cryst. Growth*, **256**, 83 (2003).
84. D. P. Macwan, C. Balasubramanian, P. N. Dave and S. Chaturvedi, *J. Saudi Chem. Soc.*, **18**, 234 (2014).
85. Q. Zhang and C. Li, *Nanomaterials*, **10**, 911 (2020).
86. X. Chen and S. S. Mao, *Chem. Rev.*, **107**, 2891 (2007).
87. X. Feng, J. Zhai and L. Jiang, *Angew. Chem. Int. Ed. Engl.*, **44**, 5115 (2005).
88. S. Y. Chae, M. K. Park, S. K. Lee, T. Y. Kim, S. K. Kim and W. I. Lee, *Chem. Mater.*, **15**, 3326 (2003).
89. Z. Yang, D. Choi, S. Kerisit, K. M. Rosso, D. Wang, J. Zhang, G. Graff and W. J. Liu, *J. Power Sources*, **192**, 588 (2009).
90. G. Dawson, W. Chen, T. Zhang, Z. Chen and X. Cheng, *Solid State Sci.*, **12**, 2170 (2010).

91. J. Yan, S. Feng, H. Lu, J. Wang, J. Zheng, J. Zhao, L. Li and Z. Zhu, *Mater. Sci. Eng. B.*, **172**, 114 (2010).
92. S. Mozia, *Cat. Today*, **156**, 198 (2010).
93. S. Y. Chae, M. K. Park, S. K. Lee, T. Y. Kim, S. K. Kim and W. I. Lee, *Chem. Mater.*, **15**, 3326 (2003).
94. G. S. Falk, M. Borlaf, M. J. López-Muñoz, J. C. Fariñas, J. B. Rodriges Neto and R. Moreno, *J. Nanopart. Res.*, **20**, 1 (2018).
95. I. F. Mironyuk, L. M. Soltys, T. R. Tatarchuk and Kh. O. Savka, *Phys. Chem. Solid State.*, **21**, 462 (2020).
96. A. Athawale, A. Bokare, H. Singh, V.-H. Nguyen, D.-V. N. Vo, D. Kumar and A. Sharma., *Top. Cat.*, **63**, 1056 (2020).
97. A. J. Moreira, O. C. Lilian, P. M. Caroline, J. A. Maldi, A. D. Jeferson, C. P. Elaine, R. G. Tania and P. G. F. Gian, *Environ. Sci. Pollut. Res. Int.*, **27**, 27032 (2020).
98. M. Y. Nassar, E. I. Ali and E. S. Zakaria, *RSC. Adv.*, **7**, 8034 (2017).
99. S. B. Somvanshi, M. V. Khedkar, P. B. Kharat and K. M. Jadhav, *Ceram. Int.*, **46**, 8640 (2020).
100. V. A. Bharati, S. B. Somvanshi, A. V. Humbe, V. D. Murumkar, V. V. Sondur and K. M. Jadhav, *J. Alloys Compd.*, **821**, 153501 (2020).
101. D. N. Bhoyar, S. B. Somvanshi, P. B. Kharat, A. A. Pandit and K. M. Jadhav, *Phys. B.*, **581**, 411944 (2020).
102. S. B. Somwanshi, S. B. Somvanshi and P. B. KKharat, *J. Phys. Conf. S.*, **1**, 1644 (2020).
103. P. Praveen, G. Viruthagiri, S. Mugundan and N. Shanmugam, *Spectrochim. Acta A Mol. Biomol. Spectrosc.*, **117**, 622 (2014).
104. J. Wei, L. Zhao, Suili Peng, J. Shi, Z. Liu and W. Wen, *J. Sol Gel Sci. Technol.*, **47**, 311 (2008).
105. A. Kathiravan and R. Renganathan, *J. Colloid Interface Sci.*, **335**, 196 (2009).
106. K. Olurode, G. M. Neelgund, A. Oki and Z. Luo, *Spectrochim. Acta A Mol. Biomol. Spectrosc.*, **89**, 333 (2012).
107. X. Lu, Xiuqian Lv, Z. Sun and Y. Zheng, *Eur. Polym. J.*, **44**, 2476 (2008).
108. A. Ranga Rao and V. Dutta, *Sol. Energy Mater. Sol. Cells.*, **91**, 1075 (2007).
109. A. Keiteb, E. Saion, A. Zakaria, N. Soltani and N. Abdullahi, *Appl. Sci.*, **6**, 295 (2016).
110. S. A. Gene, E. Saion, A. H. Shaari, M. A. Kamarudin, N. M. Al-Hada and A. Kharazmi, *J. Nanomater.*, **2014**, 1 (2014).
111. S. Kumar, S. Jain, B. Y. Yadav Lamba and P. Kumar, *Sol. Energy*, **159**, 423 (2018).
112. *Mechanism of Photocatalyst*, Nippon Jitsugyo Publishing Co, Ltd (2000).
113. F. Z. Haque, R. Nandanwar and P. Singh, *Optik.*, **128**, 191 (2017).
114. M. K. Tariq, A. Riaz, R. Khan, A. Wajid, H.-U. Haq, S. Javed, M. A. Akram and M. Islam, *Mater. Res. Express.*, **6**, 106435 (2019).
115. R. F. Peters, P. A. Mantey Dos Santos, Tiele C. Machado, D. Antonio Rodriguez Lopez, Ê. L. Machado, A. de Assis and L. Rodriguez, *Eclética Quim.*, **43**, 26 (2018).
116. N. H. Harun, M. N. A. Rahman, W. F. W. Kamarudin, Z. Irwan, A. Muhammud, N. E. F. M. Akhir, M. R. Yaafar and J. Fundam. *Appl. Sci.*, **10**, 832 (2018).
117. N. Padmavathy, B. N. Murthy and K. H. Hemakumar, *J. Phys. Conf. S.*, **1**, 012044 (2021).
118. A. Ajmal, I. Majeed, R. N. Malik, M. Iqbal, M. Arif Nadeem, I. Hussain, S. Yousaf, Zeshan, G. Mustafa, M. I. Zafar and M. Amtiaz Nadeem, *J. Environ. Chem. Eng.*, **4**, 2138 (2016).
119. A. A. Isari, A. Payan, M. Fattahi, S. Jorfi and B. Kakavandi, *Appl. Surf. Sci.*, **462**, 549 (2018).
120. V. R. Posa, V. Annavaram, J. R. Koduru, P. Bobbala, M. V. and A. R. Somala, *J. Exp. Nanosci.*, **11**, 722 (2016).
121. R. Velmurugan, B. Krishnakumar, R. Kumar and M. Swaminathan, *Arab. J. Chem.*, **5**, 447 (2012).
122. F. D. Mai, C. S. Lu, C. W. Wu, C. H. Huang, J. Y. Chen and C. C. Chen, *Sep. Purif. Technol.*, **62**, 423 (2008).
123. N. C. Joshi and P. Gururani, *Curr. Res. Green Sustain. Chem.*, **5**, 100306 (2022).
124. O. Deflaoui, A. Boudjemaa, B. Sabrina, B. Hayoun, M. Bourouina and S. Bourouina-Bacha, *React. Kinet. Mech. Cat.*, **133**, 1141 (2021).
125. M. Kocijan, L. Ćurković, D. Ljubas, K. Mužina, I. Bačić, T. Radošević, M. Podlogar, I. Bdikin, G. Otero-Irurueta, M. J. Hortigüela and G. Gonçalves, *Appl. Sci.*, **11**, 3966 (2021).
126. S. Bibi, A. Ahmad, M. A. R. Anjum, A. Haleem, M. Siddiq, S. S. Shah and A. A. Kahtani, *J. Environ. Chem. Eng.*, **9**, 105580 (2021).
127. N. Prabhakarrao, T. S. Rao, K. V. D. Lakshmi, G. Divya, G. Jaishree, I. M. Raju and S. Abdul Alim, *Sustain. Environ. Res.*, **31**, 1 (2021).
128. P. Parthipan, M. A. Al-Dosary, A. A. Al-Ghamdi and A. Subramania, *J. King Saud Univ. Sci.*, **33**, 101438 (2021).
129. S. Zarrin and F. Heshmatpour, *J. Hazard. Mater.*, **351**, 147 (2018).
130. M. Kocijan, L. Ćurković, D. Ljubas, K. Mužina, I. Bačić, T. Radošević, M. Podlogar, I. Bdikin, G. Otero-Irurueta, M. J. Hortigüela and G. Gonçalves, *Appl. Sci.*, **11**, 3966 (2021).
131. Y. Panahian and N. Arsalani, *J. Phys. Chem. A.*, **121**, 5614(2017).
132. H. Soni, N. Kumar, K. Patel and R. Kumar, *Int. J. Recent Res. Rev.*, **7**, 10 (2014).
133. M. Rahbar and Mohsen Behpour, *J. Mater. Sci. Mater. Electron.*, **27**, 8348 (2016).
134. M. Pérez-González, S. A. Tomás, J. Santoyo-Salazar and M. Morales-Luna, *Ceram. Int.*, **43**, 8831 (2017).
135. Y. Ren, Z. Xia, Y. Yu, X. Bai, Y. Liang, H. Wang, N. Wang, W. Jiang, S. Liu, C. Liu, W. Ding, Z. Zhang and C. Dong, *Opt. Mater.*, **128**, 112440 (2022).
136. A. S. Alkorbi, H. Muhammad Asif Javed, S. Hussain, S. Latif, M. S. Mahr, M. S. Mustafa, R. Alsaiari and N. A. Alhemiary, *Opt. Mater.*, **127**, 112259 (2022).
137. Y. Li, X. Zhang, X. Hu, Z. Li, J. Fan and E. Liu, *Opt. Mater.*, **127**, 112252 (2022).
138. J. Hou, L. Kong, Y. Xie, J. Ma, Y. Liu, M. Chen and Q. Wang, *Ceram. Int.*, **42**, 3941 (2022).
139. J. Ma, J. Dai, Y. Duan, J. Zhang, L. Qiang and J. Xue, *Renew. Energy*, **156**, 1008 (2020).
140. N. Qutub, P. Singh, S. Sabir, S. Sagadevan and W. C. Oh, *Sci. Rep.*, **12**, 5759 (2022).
141. J. Yu, Z. Pang, C. Zheng, T. Zhou, J. Zhang, H. Zhou and Q. Wei, *Appl. Surf. Sci.*, **470**, 84 (2019).
142. T. Zhou, L. Ma, M. Gan, H. Wang and C. Hao, *J. Phys. Chem. Solids.*, **125**, 123 (2019).
143. K. R. Reddy, K. V. Karthik, S. B. B. Prasad, S. K. Soni, H. M. Jeong and A. V. Raghu, *Polyhedron*, **120**, 169 (2016).
144. H. Zhang, Z. Tao, Y. Tang, M. Yang and G. Wang, *New J. Chem.*,

40, 8587 (2016).
145. N. Güy, K. Atacan, B. Boutra and M. Özacar, *Water Sci. Technol.*, **82**, 1912 (2020).
146. Y. Zheng, H. Qi, L. Zhang, Y. Zhang, L. Zhong, X. Zhang, Y. Feng and J. Xue, *Water Sci. Technol.*, **85**, 2625 (2022).
147. E. T. Helmy and E. Gomaa, *J. Water Environ. Nanotechnol.*, **3**, 116 (2018).
148. J. Zhang, X. Liu, T. Ye, G. Zheng, X. Zheng, P. Liu and X. Guan, *J. Alloys Compd.*, **698**, 819 (2017).
149. Z. Siraj, I. M. Maafa, I. Shafiq, N. Shezad, P. Akhter, W. Yang and M. Hussain, *Environ. Sci. Pollut. Res. Int.*, **28**, 53340 (2021).
150. N. Raza, W. Raza, H. Gul, M. Azam, J. Lee, K. Vikrant and K. Kim, *J. Cleaner Prod.*, **254**, 120031 (2020).
151. Y.-J. Lee, H. S. Lee, C.-G. Lee, S.-J. Park, J. Lee, S. Jung and G.-A. Shin, *Appl. Sci.*, **10**, 6710 (2020).
152. M. Kowalska, M. Woźniak, M. Kijek, P. Mitrosz, J. Szakiel and P. Turek, *Sci. Rep.*, **12**, 1 (2022).
153. L. E. Nd. de Castro, E. C. Meurer, H. J. Alves, M. A. Santos, E. Vasques and L. M. S. Colpini, *Braz. Arch. Biol. Technol.*, **63**, 1 (2020).
154. C. Ram, R. K. Pareek and V. Singh, *Int. J. Theor. Appl. Sci.*, **4**, 82 (2012).
155. Z. Mohammed Redha, H. Abdulla Yusuf, R. Amin and M. Bououdina, *Arab J. Basic Appl. Sci.*, **27**, 287 (2020).
156. A. A. Noaman, *Egypt. J. Chem.*, **64**, 4351 (2021).
157. N. M. Almhana, S. Z. Al-Najjar, Z. A. Naser, Z. T. Al-Sharify and T. H. Nail, *Egypt. J. Chem.*, **65**, 481 (2022).
158. M. Kulkarni and P. Thakur, *Int. J. Eng. Res. Gen. Sci.*, **2**, 245 (2014).
159. P. Trivedi and S. Sharma, *Int. J. Sci. Res.*, **8**, 60 (2019).
160. W. Rezig and M. Hadjel, *Orient. J. Chem.*, **30**, 993 (2014).
161. A. Stoyanova, A. Bachvarova-Nedelcheva and Reni Iordanova, *J. Chem. Technol. Metall.*, **53**, 1173 (2018).
162. A. Giwa, P. O. Nkeonye, K. A. Bello, E. G. Kolawole and A. O. Campos, *Int. J. Appl.*, **2**, 90 (2012).
163. H. Fu, M. Gong, X. Ning, X. Yang, X. An, Q. Zou, S. Xiong and D. Han, *Powder Technol.*, **376**, 593 (2020).
164. H. Anwer, A. Mahmood, J. Lee, K. Kim, J. Park and A. C. K. Yip, *Nano Res.*, **12**, 955 (2019).
165. Md. A. I. Molla, I. Tateishi, M. Furukawa, H. Katsumata, T. Suzuki and S. Kaneco, *Open J. Inorg. Non Metallic Mater.*, **7**, 1 (2017).
166. L. Pan, J. Zou, X. Liu, X. Liu, S. Wang, X. Zhang and L. Wang, *Ind. Eng. Chem. Res.*, **51**, 12782 (2012).
167. A. J. Nozik and R. Memming, *J. Phys. Chem.*, **100**, 13061 (1996).
168. Y. Su, L. Peng, J. Guo, S. Huang, L. Lv and X. Wang, *J. Phys. Chem. C.*, **118**, 10728 (2014).
169. A. Fujishima, T. N. Rao and D. A. Tryk, *J. Photochem. Photobiol. C.*, **1**, 1 (2000).
170. W. J. Kim, D. Pradhan, B.-K. Min and Y. Sohn, *Appl. Cat. B.*, **147**, 711 (2014).